RSC Advances

PAPER

View Article Online
View Journal | View Issue

Cite this: *RSC Adv.*, 2025, **15**, 5932

Aggregation-induced enhanced emission (AIEE), pH sensing and selective detection of sulfuric acid of novel imidazole-based surrogates made *via* microwave-assisted synthesis†

Noorullah Baig, [ab] Suchetha Shetty, [ab] Anuvasita Parikh,[c] Ajay K. Sah[c] and Bassam Alameddine *[ab]

A novel series of imidazole derivatives (**4a–d**) was synthesized *via* a microwave-assisted synthesis and whose structures were elucidated using ^{1}H and ^{13}C NMR, ESI-HRMS, and FT-IR spectroscopy. Photophysical characterization revealed absorption peaks around 305 nm and 327–365 nm, with strong photoluminescence (PL) emission maxima ranging between 435 and 453 nm. Aggregation-induced enhanced emission (AIEE) behavior was observed in THF/H_2O mixtures, where **4a–c** showed maximal fluorescence at certain solvent ratios, indicating aggregate formation. **4d** disclosed a wavelength shift from 408 to 460 nm along with an enhanced emission, which is attributed to restricted intramolecular rotation (RIR), as confirmed by viscosity studies. Fluorescence lifetime and dynamic light scattering (DLS) measurements further supported the aggregation process, with particle sizes between 100 nm and 720 nm. Density functional theory (DFT) calculations validated electronic conjugation, showing HOMO–LUMO bandgaps (ΔE) of approximately 2.01–2.23 eV for **4a–d**. Compound **4a** exhibited the largest HOMO–LUMO energy gap of 2.23 eV, indicating greater electronic stability and enhanced emission efficiency upon aggregation. In contrast, compound **4d**, with the smallest energy gap of 2.01 eV, suggests higher reactivity and better sensitivity to aggregation phenomena. This characteristic renders **4d** particularly advantageous for sensing applications where rapid responsiveness to environmental variations is critical. pH sensing studies demonstrated the stability of **4a–d** over a broad pH range, with **4d** showing a 47 nm red shift in highly acidic conditions besides a selectivity for sulfuric acid detection. Investigation of sulfuric acid detection limit was studied, revealing a capacity for **4a–d** to detect an acidic concentration as low as 16.5 μM. Stability and practical applicability of **4d** compound as a sensor are further confirmed through reversibility and repeatability tests which reveal the possibility to regenerate the imidazole derivative even after several uses.

Received 3rd February 2025
Accepted 17th February 2025

DOI: 10.1039/d5ra00786k

rsc.li/rsc-advances

Introduction

Imidazole derivatives, which are considered among the most nitrogen-abundant heterocycles, are commonly found in natural products and pharmaceutical active ingredients.[1,2] These compounds are also conspicuous for their biological activities allowing for their usage in myriad applications, among others, anticancer, antimicrobial, antihypertensive, and protein kinase inhibition.[3–6] In addition to their biological properties, imidazole surrogates were reported as prominent light emitters, promoting them for potential applications in myriad fields, namely, metal sensing,[7,8] biological imaging,[9–11] LysoTracking,[12] and as components in organic light-emitting diodes (OLEDs).[13–15]

Aggregation-induced enhanced emission (AIE), a riveting photophysical phenomenon, was first discovered and presented by Tang *et al.* in 2001.[16] Since then, AIE has garnered increasing consideration for the development of efficient fluorogens, given its unique characteristics where, as opposed to traditional molecules that exhibit aggregation-caused quenching (ACQ), AIE fluorogens demonstrate weak or no emission in solution due to intramolecular motions but portray a pronounced fluorescence upon aggregation due to the restriction of these

[a]*Department of Mathematics and Natural Sciences, Gulf University for Science and Technology, Mubarak Al-Abdullah, Hawally 32093, Kuwait. E-mail: mohammad.n@gust.edu.kw; suchetha.s@gust.edu.kw; alameddine.b@gust.edu.kw*

[b]*Functional Materials Group, Gulf University for Science and Technology, Mubarak Al-Abdullah, Hawally, 32093, Kuwait*

[c]*Department of Chemistry, Birla Institute of Technology and Science, Pilani; Pilani Campus, Rajasthan 333031, India. E-mail: P20190405@pilani.bits-pilani.ac.in; asah@pilani.bits-pilani.ac.in; Tel: +965 2530 7476*

† Electronic supplementary information (ESI) available: Experimental procedure, characterization of all compounds, and copies of NMR, EI-HRMS, FT-IR, UV-vis absorption and Emission spectra and AIE studies. See DOI: https://doi.org/10.1039/d5ra00786k

motions.[17] On the other hand, aggregation-induced enhanced emission (AIEE) is a photophysical phenomenon where aggregates of a given emissive compound display an increased fluorescence intensity.[18] Both AIE and AIEE fluorogens are bestowed by their structural modularity, emission tunability, and biocompatibility, therefore, leading to their use in optoelectronic devices,[19] bioimaging,[20,21] stimuli-responsive materials,[22] biological applications,[23] and chemical sensing.[18,24] The latter application has witnessed extensive research to develop AIEE sensors of various ions and molecules,[24] aiming to make chemosensors with high selectivity, cost-effectiveness, and ease of preparation remains an exciting area of research.[25]

Since Sørenson's first pH measurement in 1909, the quest for more selective proton detectors continues to intrigue chemists.[26] pH is a crucial parameter in both chemical and biological systems, with enzymatic reactions and cellular buffering systems operating within narrow pH ranges.[27] Deviations in pH can signal conditions like the acidic environment of cancer cells, consequently, making pH monitoring critical in biological research.[28] Advances in the design of novel pH sensors have paved the way for the synthesis of intricate bioengineered and nanosized systems capable of non-invasive, *in situ* analysis.[29]

Additionally, sulfuric acid has a wide range of industrial applications, with its primary use being in the production of fertilizers.[30] This oxidizing agent is also employed as a key reagent in the synthesis of other chemical compounds, such as, hydrochloric acid, nitric acid, sulfate salts, detergents, and pharmaceuticals.[31] Due to its extensive usage, the precise detection of sulfuric acid deems essential to monitor the environment, maintain the product quality and ensure safety during industrial processing. Recent advancements in optical fiber technology has significantly improved chemical sensing, making them invaluable sulfuric acid detectors.[32,33]

In this work, we report the synthesis of a new series of imidazole derivatives **4a–d**, which were made by reacting a specially designed benzil derivative, decorated with lateral bulky groups **2**, with various commercially available mono- and di-benzaldehydes by a simple microwave-assisted one-pot synthesis. **4a–d** were subsequently explored as AIEE fluorogens, pH fluorosensors, and selective sensors of sulfuric acid. To the best of our knowledge, this is the first report which explores the employment of such imidazole compounds bearing bulky lateral groups as AIEE fluorogens and chemical sensors.

Results and discussion

Synthesis

Target imidazoles **4a–d** were made by attaching the 4-*tert*-butylphenylacetylene **1** group to the extremities of the commercially available 1,2-bis(4-bromophenyl)ethane-1,2-dione (DBB), through a dual Pd-catalyzed Sonogashira cross-coupling reaction, yielding 1,2-bis(4-((4-(*tert*-butyl)phenyl) ethynyl)phenyl)ethane-1,2-dione **2** with an excellent yield of 90% (Scheme S1 of the ESI file†).[34,35] Subsequently, a microwave-assisted, catalyst-free, one-pot reaction between compound **2** and the commercially available mono- (**3a-b**) and di-aldehydes (**3c**) at 180 °C in the presence of ammonium acetate (NH_4OAc) afforded the target imidazoles **4a–d** within 10 minutes of reaction (Scheme 1). **4a–d** exhibited high solubility in common organic solvents, including chloroform, DCM, and THF, which allowed for their seamless structural analysis using ^{1}H- and ^{13}C-NMR spectroscopy, high-resolution mass spectrometry (ESI-HRMS), and FT-IR spectroscopy (see Fig. S1–S5, S6–S10, S11–S15 and S16–S20 in the ESI file†).

The ^{1}H-NMR spectra of **4a–d** exhibit a distinct, high-intensity signal in the aliphatic region between 1.28 and 1.36 ppm, thus indicating the presence of the *tert*-butyl groups. The proton signals of the aromatic regions for **4a–d** appear in the range of 7.95 and 7.32 ppm (see Fig. S1–S5 in the ESI file†). ^{13}C-NMR spectra disclose the aromatic carbon signals for **4a–d** between 151.85 and 119.97 ppm, with additional characteristic signals at ~88.65, ~34.7 and ~31.1 ppm, which are attributed to the fingerprint peaks of sp and sp^3 hybridized carbons of the alkynyl and tertiary butyl groups, respectively (see Fig. S6–S10 in the ESI file†).

Electrospray ionization high-resolution mass spectrometry (ESI-HRMS) further confirms the formation of **4a–d**, divulging the exact mass peaks for **4a–d** which correspond to the calculated values for each compound (see Fig. S11–S15 in the ESI file†). FT-IR spectra of **4a–d** also exhibit the anticipated stretching and bending vibrations for the key functional groups, including C≡C, (2000–2219 cm^{-1}) C–H, (2951–2958 cm^{-1}; 828–836 cm^{-1} ben) C=C, (1488–1514 cm^{-1}) and C–N, (1102–1105 cm^{-1}) therefore, further substantiating the successful synthesis of the target compounds (see Fig. S16–S20 in the ESI file†).

Photophysical properties

The photophysical properties of compounds **4a–d** were examined using UV-vis absorption and emission spectroscopy in THF as a solvent. Fig. 1 portrays the absorbance of compounds **4a–d** which display two peaks, the first ranging between 300 and 305 nm, whereas the second is detected in the range of 327–365 nm and which corresponds to the π–π* transitions of the target compounds' aromatic cores.[36]

Photoluminescence (PL) measurements of **4a–d** were conducted in the same solvent portraying similar emission peaks for **4a–c** with a λ_{max} in the range of 428 to 435 nm. Interestingly, **4d**, which contains a diimidazole core, exhibits two distinct emission peaks at approximately 428 and 453 nm.[37]

Aggregation-induced enhanced emission (AIEE) studies

The newly synthesized imidazole derivatives **4a–d**, featuring multiple rotational centers, are anticipated to exhibit aggregation-induced enhanced emission (AIEE) due to revolving restriction of the peripheral phenyl rings, which diminishes luminescence in solution.[38] Compounds **4a–d** are highly soluble in THF but insoluble in water thus making THF/H_2O mixtures ideal for exploring their AIEE behavior (see Fig. 2 and S21–S23 in the ESI file†). Solutions of **4a–d** in neat THF show weak emission peaks but whose fluorescence intensities increase as the water fraction (f_w) soars, suggesting the

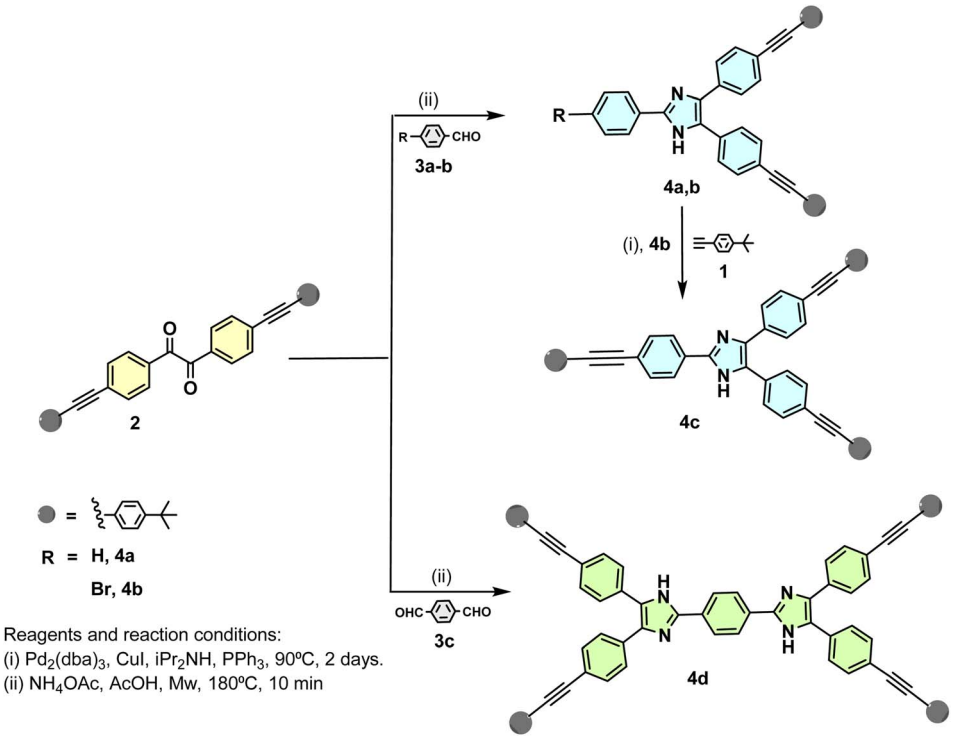

Scheme 1 Synthesis of **4a–d**.

formation of aggregates prompted by the addition of water (see Fig. 2 and S21–S23 in the ESI file†). While **4a** portrays its fluorescence maximum intensity at a THF/H_2O ratio of 40 : 60, **4b,c** disclose it at a ratio of 30 : 70, before the emission starts to diminish at higher f_w. The enhancement in photoluminescence (PL) intensity at 60–70% f_w confirms the AIEE effect for targets **4a–c** and which could be explained by the interlocked networks formed by the rotationally restricted aromatic groups through the pending lateral groups linkers upon aggregation.[39] It is worthwhile to mention that the decline in PL intensity for **4a–c** when f_w > 60% or 70% can be explained by two factors: (i) the formation of large aggregates where only the molecules present at the surface emit light upon excitation, thus, resulting in the decrease of the overall fluorescence intensity,[40] or (ii) the solute molecules aggregate in amorphous nanoparticle forms, therefore, leading to a reduction in the emission intensity, unlike the enhancement observed with the formation of crystalline nanoparticles.[41] However, in instances where higher f_w did not prompt precipitation, this could be explained by the formation of aggregates whose size remains at the nanoscale level.

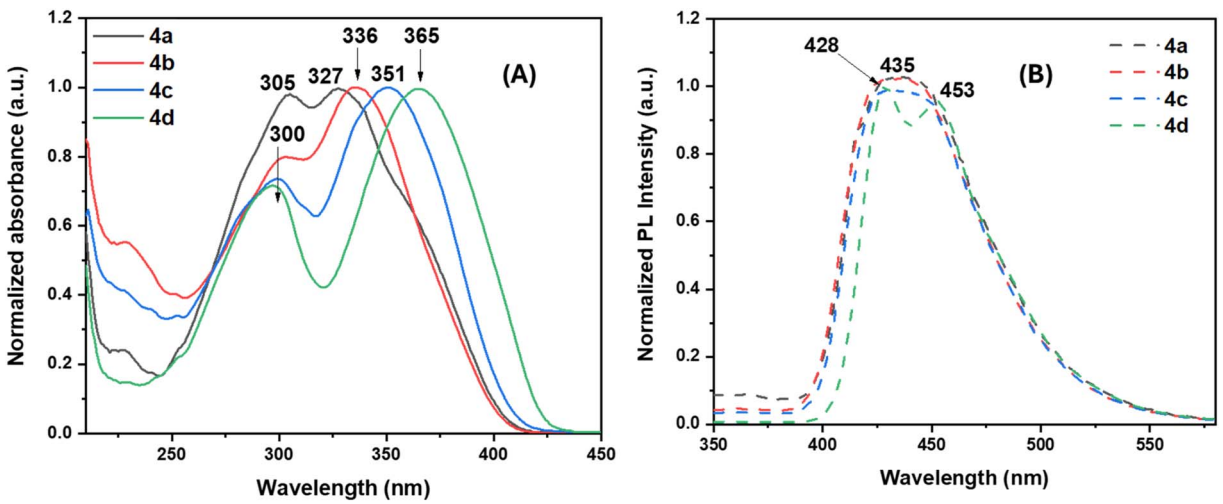

Fig. 1 Normalized UV/vis absorption (A) ($C_M = 10^{-6}$ M solid lines) and emission (B) ($C_M = 10^{-7}$ M dashed lines) spectra of compounds **4a–d** recorded in THF (absorption maxima were used as the excitation wavelengths).

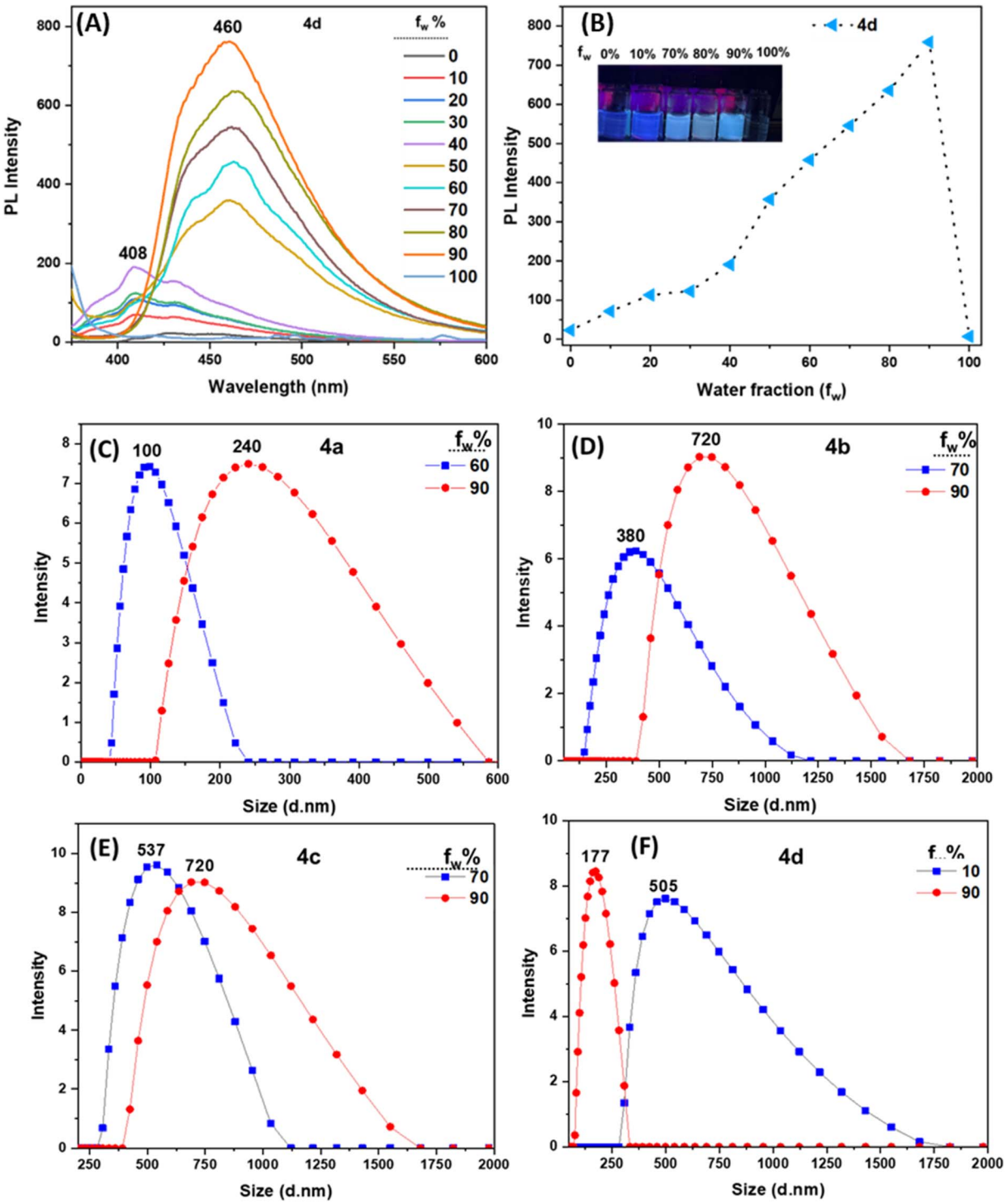

Fig. 2 (A) Emission spectra of **4d** in THF/water mixtures (0–100%); (B) plot of maximum emission intensity of **4d** *versus* water fraction; (C–F) dynamic light-scattering (DLS) spectra of **4a–d** in THF/water, at specific f_w ratio.

Dynamic light scattering (DLS) analysis of **4a–c** in THF/H_2O, specifically in solutions **4a** with f_w of 60% and 90%, **4b** 70% and 90%, and **4c** 70% and 90% discloses average aggregate sizes of approximately 100 d.nm and 240 d.nm, for **4a**, 380 d.nm and 720 d.nm, for **4b**, 537 d.nm and 720 d.nm, for **4c** (Fig. 2C–E). By correlating these findings with the change in the emission intensity observed (*c.f.* Fig. S21–S23 in the ESI file†), it is evident that the reduction in emission at f_w of 90% is attributed to the fact that only the molecules at the surface of large aggregates contribute in emission.[42]

On the other hand, the fluorescence intensity of compound **4d** has gradually increased from 0% to 90% in THF/H_2O mixture

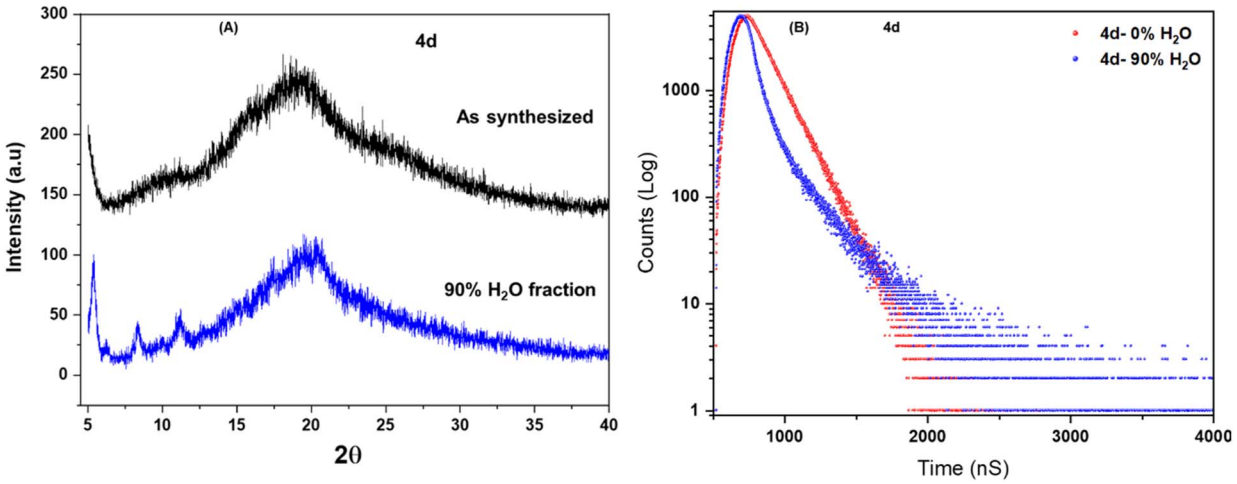

Fig. 3 (A) Powder XRD pattern of the synthesized (black graph) and THF/water, f_w 90% (blue graph) of **4d** and (B) fluorescence lifetime decay profiles of **4d** in THF/water, f_w %; 0 (red graph) and 90 (blue graph).

in addition to the emission wavelength shifts from 408 nm to 460 nm (Fig. 2A and B) This suggests that the mechanism of the AIE activity of **4d** is mainly through restricted intramolecular rotation (RIR) which was further supported by recording the emission spectra of **4d** with different mixtures of THF and high viscous solvent polyethylene glycol (PEG) 0–90% (with a fixed amount of THF and a gradually increasing amount of PEG) (see Fig. S24 in the ESI file†). The emission intensity was gradually enhanced by increasing the viscosity. The viscosity experiments indicates that AIEE in **4d** is due to the RIR mechanism.[43,44]

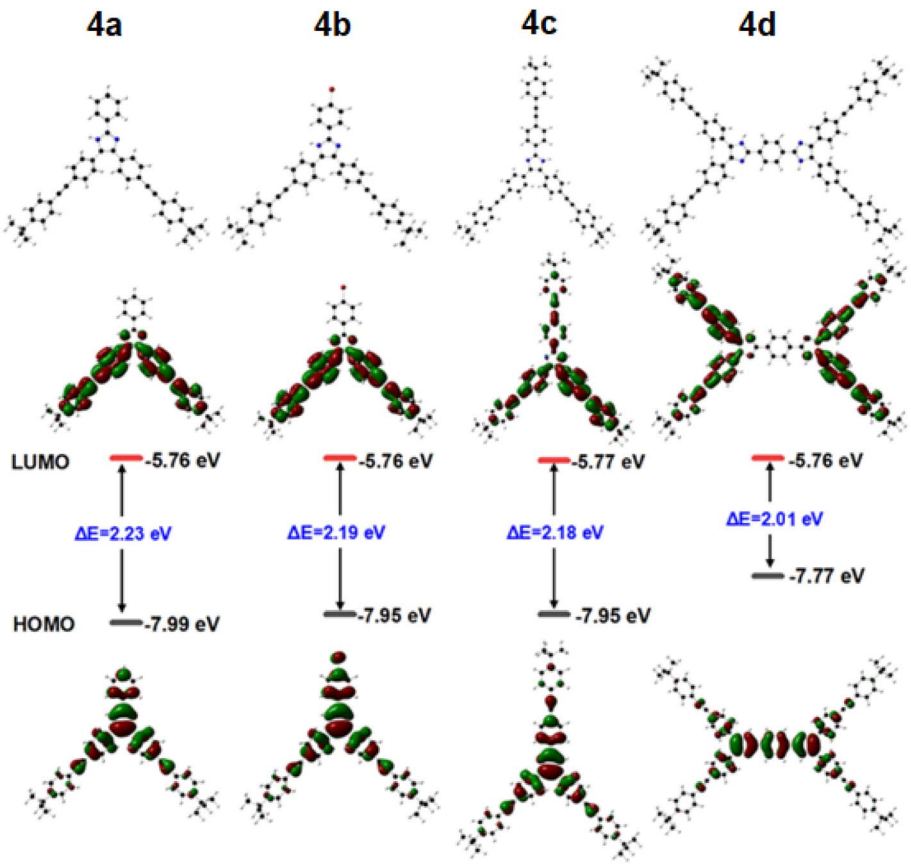

Fig. 4 The optimized structures and molecular orbital amplitude plots of HOMO and LUMO energy levels for **4a–d** computed using the B3LYP/6-31G* basis set.

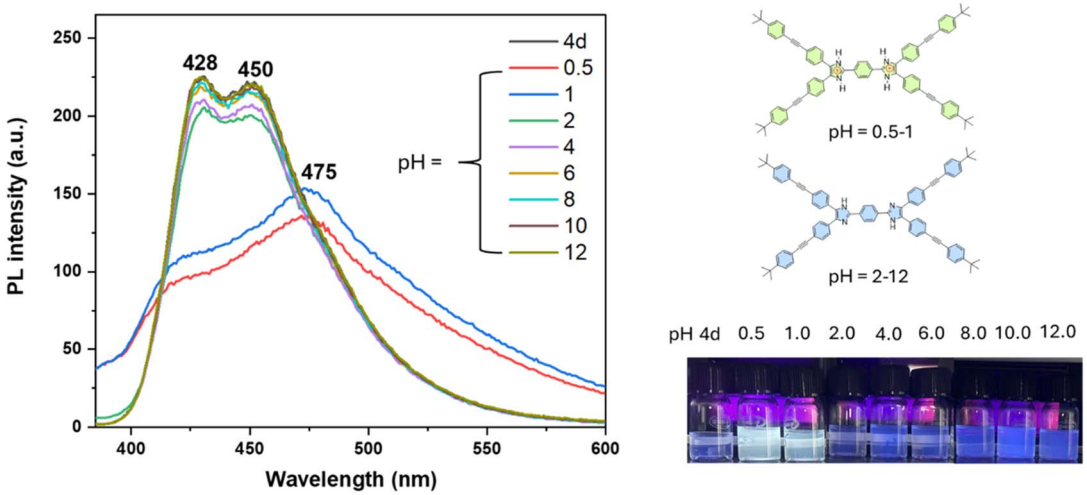

Fig. 5 Emission spectra of **4d** (1×10^{-7} M) in different THF-buffer mixture, 9 : 1, v/v, $\lambda_{exc} = 365$ nm.

Dynamic light scattering (DLS) analysis of **4d** in THF/H_2O, with f_w of 10% and 90%, discloses average aggregate sizes of approximately 505 d.nm and 177 d.nm, respectively (Fig. 2F).

Furthermore, powder X-ray diffraction (PXRD) of **4d** as synthesized and that of the 90% water fraction solutions were investigated where an aliquot of the latter was centrifuged and filtered before collecting the residue which was collected and then characterized. PXRD analysis revealed broad peaks for **4d**, indicating its amorphous nature, contrarily to the sharp and intense diffraction peaks for the isolated sample of **4d** from solution, thus, indicating microsegregation (Fig. 3A), and which further supports the RIR effect leading to an increase in the PL intensity with an increasing water concentration.

The lifetimes of compounds **4a–d** were measured at room temperature employing time-correlated single photon counting (TCSPC). Samples **4a–c**, prepared in THF/H_2O mixtures with concentration ratios of 40 : 60, 30 : 70, and 30 : 70, respectively, were found to have determined lifetimes of 1.48, 1.46, and 1.14 ns, respectively (see Fig. S25 in the ESI file†). In contrast, the lifetime of **4d** measured in pure THF was 0.32 ns, while a notable increase to 1.05 ns was observed for the same derivative in a 10 : 90 THF/H_2O mixture, which undoubtedly indicates enhanced luminescence yield due to aggregation effects when compared to **4d** solution in pure THF (Fig. 3B).[45]

Electronic structure

Computational optimization of **4a–d** using B3LYP/6-31G* basis set disclose similar orbital distribution of their HOMO–LUMO energy levels with electron conjugation majorly located in the benzene rings connected through the alkynyl bonds at the HOMO level, and which becomes more relevant in the remaining part of the target compound at the LUMO level. All

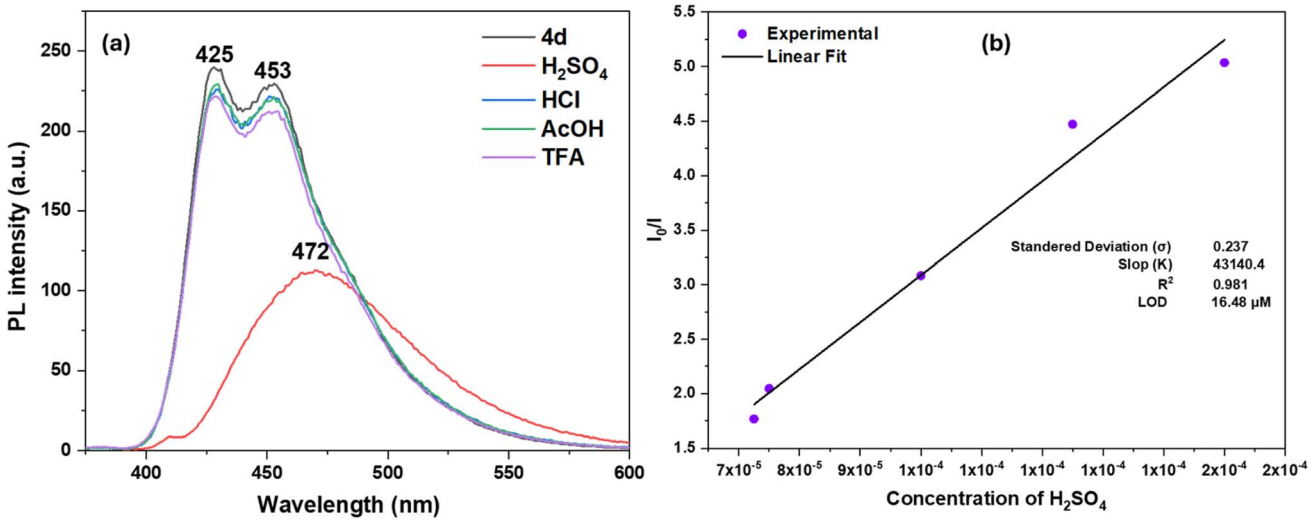

Fig. 6 (a) Emission spectra of **4d** (1×10^{-6} M in THF) in various acid solutions (excitation wavelength: 365 nm). (b) Linear correlation of I_0/I *vs.* the concentrations of H_2SO_4 in the range 0.5×10^{-5} to 1.75×10^{-4} M.

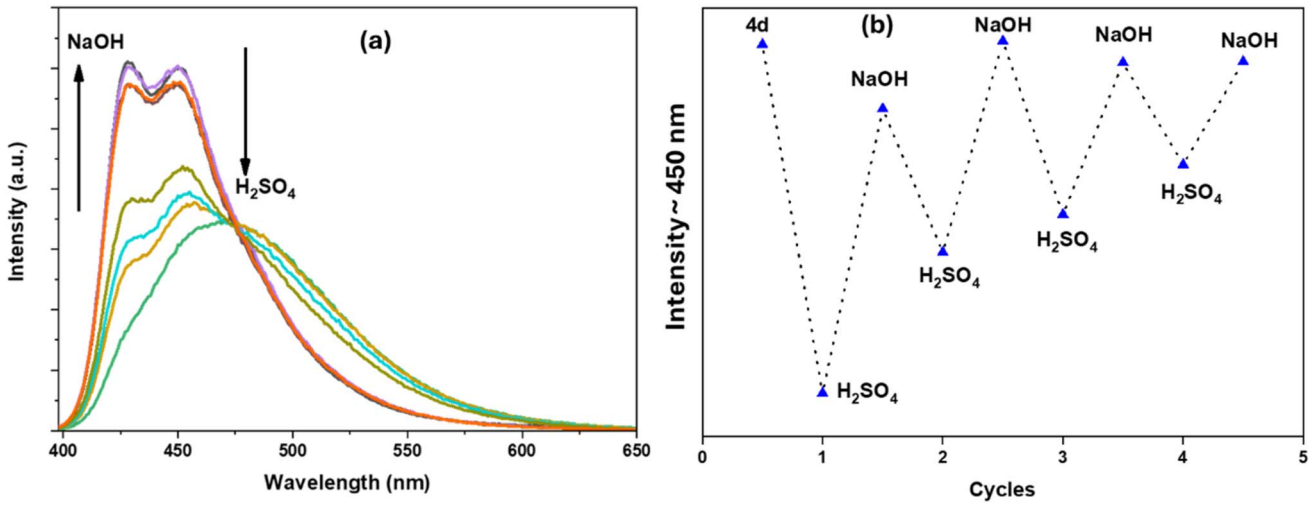

Fig. 7 (a) Emission spectra of **4d** (1×10^{-6} M in THF) in different acidic and basic solutions (excitation wavelength: 365 nm). (b) Change of the emission intensity at ~450 nm upon adding H_2SO_4 and NaOH (excitation wavelength: 365 nm).

the structures were found to be deviated from planarity, especially at the aryl-imidazole connection by a dihedral angle of around 6.2° to 6.3°, which prevents their effective conjugation (Fig. 4). Examination of the HOMO, LUMO, and energy variance values for the four samples **4a–d** offers valuable insights into their properties as prominent Aggregation-Induced Emission (AIE) materials, with HOMO energies ranging from −7.99 eV to −7.77 eV, thus indicating that these compounds possess relatively high energy levels for the highest occupied molecular orbital. In contrast, the calculated LUMO energies were found at −5.76 eV to −5.77 eV. Therefore, the HOMO–LUMO energy differences are found in the range of 2.01 eV to 2.23 eV. Sample **4a** has disclosed the largest HOMO–LUMO gap of 2.23 eV, suggesting larger stability and enhanced emission properties upon aggregation,[46] as such a large gap is expected to reduce non-radiative decay thus allowing for more efficient luminescence, a critical characteristic of AIE materials.[47] On the other hand, **4d** which exhibits the smallest energy difference of 2.01 eV, may imply a higher reactivity or sensitivity to aggregation conditions,[48] which could be advantageous for sensing applications where responsiveness to environmental changes is crucial. The slightly reduced energy gap in this sample may facilitate easier electronic transitions, allowing for real-time monitoring and detection capabilities.

pH sensing studies

Given that most imidazole derivatives are sensitive to acids,[49] fluorescence pH sensing studies of **4a–d** (1×10^{-7} M) were conducted in THF-buffer mixtures (9 : 1, v/v) whose pH range between 0.5 and 12.[49,50] When excited at 365 nm, **4a–c** exhibited emission bands at 435 nm, 432 nm and 430 nm, respectively, across the pH range of 1–12. Alternatively, **4d** portrayed two emission bands at 428 nm, and 450 nm, with the former maintaining this emission maximum at a pH range of 1–12 while the latter keeping its fluorescence at pH values in the range of 2 to 12. Interestingly, the emission spectra of compounds **4a–c** were red-shifted by up to 40 nm at a pH of 0.5, with quenching up to 44%. Whereas that of **4d** exhibited a more significant red shift of 47 nm with quenching up to 40% at pH values of 0.5 and 1.0 with a conspicuous color change from blue to pale yellow under UV illumination (Fig. 5). It is noteworthy that the hitherto mentioned observed red shifts are likely due to the protonation of the imine group in the imidazole skeleton.[49] These observations clearly demonstrate that compounds **4a–d** serve as effective fluorosensors at pH values ranging from 0.5 to 1 (see Fig. 5 and S26–S28 in the ESI file†).

Specific acid sensing studies

Fluorescence acid sensing experiments were performed using a 1×10^{-6} M THF solution of **4d** with 10 equivalents of four different acids, notably, trifluoroacetic acid (TFA), hydrochloric acid (HCl), acetic acid (AcOH), and sulfuric acid (H_2SO_4). A 1 : 1 (v/v) mixture of **4d** and a given acid was excited at 365 nm, portraying no change in the emission of **4d** upon using the monoprotic acids (TFA, AcOH, and HCl), unlike the diprotic sulfuric acid (H_2SO_4) which caused the emission of **4d** to be red shifted by 47 nm, additionally a hypochromic shift (Fig. 6a) strongly suggests an interaction between the latter and H_2SO_4 attributed to the protonation of the imine moiety of the imidazole.[51] Quantitative detection of H_2SO_4 was investigated employing the limit of detection (LOD), which was determined using the formula $3\sigma/K$,[52,53] where σ represents the standard deviation obtained from 10 consecutive scans of blank samples whereas K is the slope of the calibration curve. Therefore, titration studies of **4d** with H_2SO_4 were carried out utilizing a 1×10^{-3} M stock solution of **4d** in THF and aqueous H_2SO_4 solution concentrations ranging from 0.5×10^{-5} M to 1.75×10^{-4} M. During the titration, 50 μL of **4d** and 5 μL of H_2SO_4 solutions were added and diluted to a final volume of 2 mL, revealing a decrease in the emission intensity of **4d** with an increasing concentration of H_2SO_4, as expected (see Fig. S29 in the ESI file†). The calibration curve was obtained by plotting the

changes in I_0/I ratio at ~450 nm against the corresponding H_2SO_4 concentrations allowing for the calculation of the LOD and which was found to be 16.48 μM (1.62 ppm, Fig. 6b).

The stability and reproducibility of **4d** were evaluated using H_2SO_4 and NaOH. Thus, reversibility experiments were carried out by adding H_2SO_4 (1.5×10^{-4} M) and NaOH (3×10^{-4} M) successively to a 1.5×10^{-5} M solution of **4d** over four cycles and recording the fluorescence spectra during each addition step (Fig. 7). The results indicate that **4d** exhibits reversible behavior in the presence of H_2SO_4 and NaOH, thus confirming its stability.

Conclusion

In summary, a novel series of imidazole derivatives **4a–d** was successfully synthesized, displaying strong aggregation-induced enhanced emission (AIEE) photophysical properties. Computational optimization of **4a–d** using B3LYP/6-31G* basis set disclose compound **4a** exhibited the highest HOMO–LUMO energy gap (2.23 eV), suggesting enhanced electronic stability and superior emission properties upon aggregation. In contrast, the smallest gap in **4d** (2.01 eV) conferred higher sensitivity to environmental changes, making it a standout candidate for advanced sensing applications. Compounds **4a–d** demonstrated significant sensitivity to low pH environments, promoting them as promising candidates for pH-responsive applications. Additionally, specific acid sensing studies revealed that **4d** selectively interacts with sulfuric acid (H_2SO_4) with detection limit of 16.48 μM (1.62 ppm). Furthermore, stability and reusability tests confirmed the sturdiness of **4d** as a sensor even after several successive utilization cycles. These findings underscore the versatility of the reported imidazole derivatives as promising versatile materials for applications in environmental monitoring, chemical sensing, and optoelectronic technologies. The robust AIEE properties, coupled with exceptional sensitivity and selectivity, position these compounds as valuable contributors to the development of next-generation functional materials.

Data availability

The raw data required to reproduce these findings are available upon request.

Conflicts of interest

There are no conflicts to declare.

Acknowledgements

The project was partially supported by Kuwait Foundation for the Advancement of Sciences (KFAS) under project code PN17-34SC-01 and this project has been partially supported by Gulf University for Science and Technology under project code: ISG-115 We are thankful to the Birla Institute of Technology and Science, Pilani; Pilani Campus, Rajasthan, India, for providing the analytical, spectral facilities (FTIR, NMR, HRMS, DLS, and PXRD) and High-Performance Computing (HPC) center.

References

1 E. Saeedian Moghadam, F. Bonyasi, B. Bayati, M. Sadeghi Moghadam and M. Amini, Recent Advances in Design and Development of Diazole and Diazine Based Fungicides (2014–2023), *J. Agric. Food Chem.*, 2024, **72**(28), 15427–15448, DOI: **10.1021/acs.jafc.4c02187**.

2 L. Zhang, X.-M. Peng, G. L. V. Damu, R.-X. Geng and C.-H. Zhou, Comprehensive Review in Current Developments of Imidazole-Based Medicinal Chemistry, *Med. Res. Rev.*, 2014, **34**(2), 340–437, DOI: **10.1002/med.21290**.

3 R. Di Santo, A. Tafi, R. Costi, M. Botta, M. Artico, F. Corelli, M. Forte, F. Caporuscio, L. Angiolella and A. T. Palamara, Antifungal Agents. 11. N-Substituted Derivatives of 1-[(Aryl)(4-aryl-1H-pyrrol-3-yl)methyl]-1H-imidazole: Synthesis, Anti-Candida Activity, and QSAR Studies, *J. Med. Chem.*, 2005, **48**(16), 5140–5153, DOI: **10.1021/jm048997u**.

4 P. Fan-Havard, D. Capano, S. M. Smith, A. Mangia and R. H. Eng, Development of resistance in candida isolates from patients receiving prolonged antifungal therapy, *Antimicrob. Agents Chemother.*, 1991, **35**(11), 2302–2305, DOI: **10.1128/aac.35.11.2302**.

5 K.-i. Shinohara, T. Bando, S. Sasaki, Y. Sakakibara, M. Minoshima and H. Sugiyama, Antitumor activity of sequence-specific alkylating agents: Pyrolle-imidazole CBI conjugates with indole linker, *Cancer Sci.*, 2006, **97**(3), 219–225, DOI: **10.1111/j.1349-7006.2006.00158.x**.

6 P. R. Young, M. M. McLaughlin, S. Kumar, S. Kassis, M. L. Doyle, D. McNulty, T. F. Gallagher, S. Fisher, P. C. McDonnell, S. A. Carr, *et al.*, Pyridinyl Imidazole Inhibitors of p38 Mitogen-activated Protein Kinase Bind in the ATP Site, *J. Biol. Chem.*, 1997, **272**(18), 12116–12121, DOI: **10.1074/jbc.272.18.12116**.

7 Y. Sun, X. Wang, H. Li, S. Zhang and W. Niu, Mechanically Robust Photonic-Ionic Skin Cross-Linked by Metal–Imidazole Interactions, *Adv. Funct. Mater.*, 2024, 2405345, DOI: **10.1002/adfm.202405345**.

8 X. Xin, J. Ai, F. Li, J. Zhao and L. Zhang, An imidazole functionalized copper(II)-organic framework for highly selective sensing of picric acid and metal ions in water, *Appl. Organomet. Chem.*, 2020, **34**(9), e5803, DOI: **10.1002/aoc.5803**.

9 S. Gül, E. Açıkgöz, M. Çakır and N. Menges, Design and Synthesis of ESIPT-Based Imidazole Derivatives for Cell Imaging, *ACS Omega*, 2024, **9**(23), 24291–24298, DOI: **10.1021/acsomega.3c09822**.

10 P. Rajendran, P. Murugaperumal, S. Nallathambi, F. Perdih, S. Ayyanar and S. Chellappan, Performance of 4,5-diphenyl-1H-imidazole derived highly selective 'Turn-Off' fluorescent chemosensor for iron(III) ions detection and biological applications, *Luminescence*, 2024, **39**(3), e4694, DOI: **10.1002/bio.4694**.

11 Y. Tsubono, Y. Kawamoto, T. Hidaka, G. N. Pandian, K. Hashiya, T. Bando and H. Sugiyama, A Near-Infrared Fluorogenic Pyrrole–Imidazole Polyamide Probe for Live-Cell Imaging of Telomeres, *J. Am. Chem. Soc.*, 2020, **142**(41), 17356–17363, DOI: 10.1021/jacs.0c04955.

12 S. Adhikary, L. Majumder, S. Pakrashy, R. Srinath, K. Mukherjee, C. Mandal and B. Banerji, Polysubstituted Imidazoles as LysoTracker Molecules: Their Synthesis *via* Iodine/H2O and Cell-Imaging Studies, *ACS Omega*, 2020, **5**(24), 14394–14407, DOI: 10.1021/acsomega.0c00934.

13 K. Kumar and D. Thakur, Overview of imidazole-based fluorescent materials with hybridized local and charge transfer and hot-exciton pathway characteristics in excited states, *Soft Matter*, 2024, **20**(8), 1669–1688, DOI: 10.1039/D3SM01005H.

14 H. Liu, F. Liu, Z. Cheng, Y. Yan, L. Wan, Y. Hu, Y. Xu, X. Ma and P. Lu, High-Efficiency Hybrid White Organic Light-Emitting Diodes with Extremely Low Efficiency Roll-Off and Superior Color Stability Enabled by an Emitting System with Imidazole-Biphenyl Derivatives, *Adv. Opt. Mater.*, 2024, 2401424, DOI: 10.1002/adom.202401424.

15 S. R. Nayak, Shahnawaz, I. Siddiqui, J.-H. Jou, S. Patel and S. Vaidyanathan, Multifunctional 4,5-Diphenyl-1H-imidazole-Based Luminogens as Near UV/Deep Blue Emitters/Hosts for Organic Light-Emitting Diodes and Selective Picric Acid Detection, *J. Phys. Chem. C*, 2023, **127**(1), 499–515, DOI: 10.1021/acs.jpcc.2c05220.

16 J. Luo, Z. Xie, J. W. Y. Lam, L. Cheng, H. Chen, C. Qiu, H. S. Kwok, X. Zhan, Y. Liu, D. Zhu and B. Z. Tang, Aggregation-induced emission of 1-methyl-1,2,3,4,5-pentaphenylsilole, *Chem. Commun.*, 2001, (18), 1740–1741, DOI: 10.1039/B105159H.

17 Y. Duo, L. Han, Y. Yang, Z. Wang, L. Wang, J. Chen, Z. Xiang, J. Yoon, G. Luo and B. Z. Tang, Aggregation-Induced Emission Luminogen: Role in Biopsy for Precision Medicine, *Chem. Rev.*, 2024, **124**, 11242–11347, DOI: 10.1021/acs.chemrev.4c00244.

18 X. Li, D. Wang, Y. Zhang, W. Lu, S. Yang, G. Hou, Z. Zhao, H. Qin, Y. Zhang, M. Li, *et al.*, A novel aggregation-induced enhanced emission aromatic molecule: 2-aminophenylboronic acid dimer, *Chem. Sci.*, 2021, **12**(37), 12437–12444, DOI: 10.1039/D1SC03765J.

19 P. Liu, C. Chu, W. Qiu, L. Cheng, J. Gu, Z. Mao, Z. Zhao, X. He, G. Liu, C. Peng, *et al.*, 3D/4D printed versatile fibre-based wearables for embroidery, AIE-chemosensing, and unidirectional draining, *Aggregate*, 2024, **5**(3), e521, DOI: 10.1002/agt2.521.

20 W. Liu, Q. Liu, D. Wang and B. Z. Tang, Fluorescent Porous Materials Based on Aggregation-induced Emission for Biomedical Applications, *ACS Nano*, 2024, **18**(40), 27206–27229, DOI: 10.1021/acsnano.4c08882.

21 L. Yan, Y. Zhang, B. Xu and W. Tian, Fluorescent nanoparticles based on AIE fluorogens for bioimaging, *Nanoscale*, 2016, **8**(5), 2471–2487, DOI: 10.1039/C5NR05051K.

22 J.-J. Hu, W. Jiang, L. Yuan, C. Duan, Q. Yuan, Z. Long, X. Lou and F. Xia, Recent advances in stimuli-responsive theranostic systems with aggregation-induced emission characteristics, *Aggregate*, 2021, **2**(1), 48–65, DOI: 10.1002/agt2.10.

23 H. Wang, Q. Li, P. Alam, H. Bai, V. Bhalla, M. R. Bryce, M. Cao, C. Chen, S. Chen, X. Chen, *et al.*, Aggregation-Induced Emission (AIE), Life and Health, *ACS Nano*, 2023, **17**(15), 14347–14405, DOI: 10.1021/acsnano.3c03925.

24 S. Asthana, M. S. S. V. Mouli, A. Tamrakar, M. A. Wani, A. K. Mishra, R. Pandey and M. D. Pandey, Recent advances in AIEgen-based chemosensors for small molecule detection, with a focus on ion sensing, *Anal. Methods*, 2024, **16**(27), 4431–4484, DOI: 10.1039/D4AY00618F.

25 P. P. Dash, A. K. Ghosh, P. Mohanty, R. Behura, S. Behera, B. R. Jali and S. K. Sahoo, Advances on fluorescence chemosensors for selective detection of water, *Talanta*, 2024, **275**, 126089, DOI: 10.1016/j.talanta.2024.126089.

26 A. Steinegger, O. S. Wolfbeis and S. M. Borisov, Optical Sensing and Imaging of pH Values: Spectroscopies, Materials, and Applications, *Chem. Rev.*, 2020, **120**(22), 12357–12489, DOI: 10.1021/acs.chemrev.0c00451.

27 L. Di Costanzo and B. Panunzi, Visual pH Sensors: From a Chemical Perspective to New Bioengineered Materials, *Molecules*, 2021, **26**(10), 2952, DOI: 10.3390/molecules26102952.

28 J. Mandal, P. Ghorai, P. Brandão, K. Pal, P. Karmakar and A. Saha, An aminoquinoline based biocompatible fluorescent and colourimetric pH sensor designed for cancer cell discrimination, *New J. Chem.*, 2018, **42**(24), 19818–19826, DOI: 10.1039/C8NJ04753G.

29 M. Hassan Akhtar, M. Azhar Hayat Nawaz, M. Abbas, N. Liu, W. Han, Y. Lv and C. Yu, Advances in pH Sensing: From Traditional Approaches to Next-Generation Sensors in Biological Contexts, *Chem. Rec.*, 2024, **24**(7), e202300369, DOI: 10.1002/tcr.202300369.

30 A. A. Kiss, C. S. Bildea and J. Grievink, Dynamic modeling and process optimization of an industrial sulfuric acid plant, *Chem. Eng. J.*, 2010, **158**(2), 241–249, DOI: 10.1016/j.cej.2010.01.023.

31 R. Sattar Jebur and R. Hamdan Thaher, Sulfuric Acid Highly Sensitive Detection at Different Concentrations Using Photonic Crystal Fiber Sensor, *Int. J. Saf. Secur. Eng.*, 2024, **14**(2), 459–466, DOI: 10.18280/ijsse.140213.

32 L. D. Coelho, O. Gaete and N. Hanik, An algorithm for global optimization of optical communication systems, *Int. J. Electron. Commun.*, 2009, **63**(7), 541–550, DOI: 10.1016/j.aeue.2009.02.009.

33 Z. Xu, X. Chen, H. N. Kim and J. Yoon, Sensors for the optical detection of cyanide ion, *Chem. Soc. Rev.*, 2010, **39**(1), 127–137, DOI: 10.1039/B907368J.

34 N. Baig, S. Shetty, S. Abdul Wahed, A. Hassan, N. Das and B. Alameddine, Promising CO2 Capture and Effective Iodine Adsorption of Hyper-Cross-Linked Conjugated Porous Organic Polymers Prepared from a Cyclopentannulation Reaction, *ACS Appl. Mater. Interfaces*, 2024, DOI: 10.1021/acsami.4c02948.

35 N. Baig, S. Shetty, S. A. Wahed, A. Hassan, N. Das and B. Alameddine, Designing highly porous three-dimensional triazine-bearing covalent organic polymers as prominent adsorbents of carbon dioxide and iodine, *Mater. Today Chem.*, 2024, **41**, 102339, DOI: 10.1016/j.mtchem.2024.102339.

36 N. Baig, S. Shetty, R. Tiwari, S. K. Pramanik and B. Alameddine, Aggregation-Induced Emission of Contorted Polycondensed Aromatic Hydrocarbons Made by Edge Extension Using a Palladium-Catalyzed Cyclopentannulation Reaction, *ACS Omega*, 2022, **7**(49), 45732–45739, DOI: 10.1021/acsomega.2c07168.

37 J. Jayabharathi, M. Sundharesan, A. Prabhakaran and C. Karunakaran, Understanding the binding interaction of imidazole with ZnO nanomaterials and clusters, *RSC Adv.*, 2015, **5**(13), 9518–9531, DOI: 10.1039/C4RA15957H.

38 N. Baig, S. Shetty, R. Bargakshatriya, S. K. Pramanik and B. Alameddine, Exploring Cyclopentannulation as an Effective Synthetic Tool to Design Polycyclic Aromatic Hydrocarbon AIEgens for Bioimaging, *ACS Omega*, 2024, **9**(34), 36732–36740, DOI: 10.1021/acsomega.4c05526.

39 J. Mei, N. L. C. Leung, R. T. K. Kwok, J. W. Y. Lam and B. Z. Tang, Aggregation-Induced Emission: Together We Shine, United We Soar, *Chem. Rev.*, 2015, **115**(21), 11718–11940, DOI: 10.1021/acs.chemrev.5b00263.

40 P. Alam, G. Kaur, C. Climent, S. Pasha, D. Casanova, P. Alemany, A. Roy Choudhury and I. R. Laskar, New 'aggregation induced emission (AIE)' active cyclometalated iridium(iii) based phosphorescent sensors: high sensitivity for mercury(ii) ions, *Dalton Trans.*, 2014, **43**(43), 16431–16440, DOI: 10.1039/C4DT02266A.

41 J. He, B. Xu, F. Chen, H. Xia, K. Li, L. Ye and W. Tian, Aggregation-Induced Emission in the Crystals of 9,10-Distyrylanthracene Derivatives: The Essential Role of Restricted Intramolecular Torsion, *J. Phys. Chem. C*, 2009, **113**(22), 9892–9899, DOI: 10.1021/jp900205k.

42 D. Sengottuvelu, V. Kachwal, P. Raichure, T. Raghav and I. R. Laskar, Aggregation-Induced Enhanced Emission (AIEE)-Active Conjugated Mesoporous Oligomers (CMOs) with Improved Quantum Yield and Low-Cost Detection of a Trace Amount of Nitroaromatic Explosives, *ACS Appl. Mater. Interfaces*, 2020, **12**(28), 31875–31886, DOI: 10.1021/acsami.0c05273.

43 V. Kachwal, I. S. Vamsi Krishna, L. Fageria, J. Chaudhary, R. Kinkar Roy, R. Chowdhury and I. R. Laskar, Exploring the hidden potential of a benzothiazole-based Schiff-base exhibiting AIE and ESIPT and its activity in pH sensing, intracellular imaging and ultrasensitive & selective detection of aluminium (Al3+), *Analyst*, 2018, **143**(15), 3741–3748, DOI: 10.1039/C8AN00349A.

44 S. S. Pasha, H. R. Yadav, A. R. Choudhury and I. R. Laskar, Synthesis of an aggregation-induced emission (AIE) active salicylaldehyde based Schiff base: study of mechanoluminescence and sensitive Zn(ii) sensing, *J. Mater. Chem. C*, 2017, **5**(37), 9651–9658, DOI: 10.1039/C7TC03046K.

45 P. Alam, M. Karanam, D. Bandyopadhyay, A. R. Choudhury and I. R. Laskar, Aggregation-Induced Emission Activity in Iridium(III) Diimine Complexes: Investigations of Their Vapochromic Properties, *Eur. J. Inorg. Chem.*, 2014, **2014**(23), 3710–3719, DOI: 10.1002/ejic.201402222.

46 R. Srivastava and L. R. Joshi, The effect of substituted 1,2,4-triazole moiety on the emission, phosphorescent properties of the blue emitting heteroleptic iridium(iii) complexes and the OLED performance: a theoretical study, *Phys. Chem. Chem. Phys.*, 2014, **16**(32), 17284–17294, DOI: 10.1039/C4CP02368D.

47 S. Yin, Q. Peng, Z. Shuai, W. Fang, Y.-H. Wang and Y. Luo, Aggregation-enhanced luminescence and vibronic coupling of silole molecules from first principles, *Phys. Rev. B:Condens. Matter Mater. Phys.*, 2006, **73**(20), 205409, DOI: 10.1103/PhysRevB.73.205409.

48 H. Sajid, K. Ayub, M. A. Gilani and T. Mahmood, Donor-π-Acceptor N-Methyl-4,5-Diazacarbazole Based Ultra-High Performance Organic Solar Cells: A Density Functional Theory Study, *Energy Technol.*, 2023, **11**(1), 2201164, DOI: 10.1002/ente.202201164.

49 E. Parisi, E. Santagata, A. Landi, R. Centore, M. Chino and A. Carella, Strong and pH dependent fluorescence in unprecedented anthra[2,3-d]imidazole derivatives, *Dyes Pigm.*, 2025, **232**, 112440, DOI: 10.1016/j.dyepig.2024.112440.

50 P. Alam, G. Kaur, A. Sarmah, R. K. Roy, A. R. Choudhury and I. R. Laskar, Highly Selective Detection of H+ and OH– with a Single-Emissive Iridium(III) Complex: A Mild Approach to Conversion of Non-AIEE to AIEE Complex, *Organometallics*, 2015, **34**(18), 4480–4490, DOI: 10.1021/acs.organomet.5b00447.

51 S. Dhiman, N. Singla, M. Ahmad, P. Singh and S. Kumar, Protonation- and electrostatic-interaction-based fluorescence probes for the selective detection of picric acid (2,4,6-trinitrophenol) – an explosive material, *Mater. Adv.*, 2021, **2**(20), 6466–6498, DOI: 10.1039/D1MA00478F.

52 R. Singh, K. Mitra, S. Singh, S. Senapati, V. K. Patel, S. Vishwakarma, A. Kumari, J. Singh, S. K. Sen Gupta, N. Misra, *et al.*, Highly selective fluorescence 'turn off' sensing of picric acid and efficient cell labelling by water-soluble luminescent anthracene-bridged poly(N-vinyl pyrrolidone), *Analyst*, 2019, **144**(11), 3620–3634, DOI: 10.1039/C8AN02417K.

53 S. Sinha, B. Chowdhury and P. Ghosh, A Highly Sensitive ESIPT-Based Ratiometric Fluorescence Sensor for Selective Detection of Al3+, *Inorg. Chem.*, 2016, **55**(18), 9212–9220, DOI: 10.1021/acs.inorgchem.6b01170.